Contact Resistivity of Evaporated Al Contacts for Silicon Solar Cells

Kean Chern Fong, Teng Choon Kho, Andreas Fell, Evan Franklin, Ngwe Zin, Andrew W. Blakers, Keith R. McIntosh, Thomas Ratcliff, Matthew Stocks, James Bullock and Er-Chien Wang.

***Abstract*—The contact resistivity of evaporated Al on doped silicon is examined for a range of process conditions common to the fabrication of laboratory silicon solar cells. The effects of silicon surface preparation prior to evaporation, sintering temperature, the use of a shutter, and evaporation power are investigated. The presented evaporation conditions yielded the lowest published contact resistivity between Al and phosphorus doped Si over a large range of doping concentration. It is also demonstrated that a contact resistivity below 10^{-6} Ω·cm^2 can be achieved without sintering. Three-dimensional simulations are utilized to compare the obtained results for evaporated Al contacts with those for passivated contacts.**

***Index Terms*— Photovoltaic cells, silicon solar cells, contact resistance, metal contacts, simulation**

I. Introduction

The use of evaporated Al is common in high-efficiency laboratory solar cells due to its properties of having low contact resistivity, high reflectivity, enhanced passivation of oxide-coated surfaces via alnealing [1, 2], compatible with laser patterning and photolithographic patterning. It has been used as the metal contact interface in both n- and p-type high efficiency silicon solar cells [3-6].

Evaporated Al has not been adopted in cell manufacturing due to its high costs and low throughput but it could potentially be viable with the advancement of in-line evaporator systems [7].

It is generally observed that at a given doping concentration, the contact resistivity of phosphorus doped contacts is approximately 2-3 orders magnitude higher than that of boron doped contacts, attributable to a higher barrier height at the contact interface for n-type silicon.

A sintering step at a temperature between 300-500 ^{o}C is often included in Al-evaporated contacts to form intimate contact [7-9]. The sintering step is undesirable for multiple reasons: it incurs an additional processing time and cost; it requires underlying dielectric films to be compatible in maintaining electrical isolation and passivation after sintering; it increases the possibility of contaminating the silicon; and it can cause non-ideal recombination or p-n junction shunting introduced by Al spiking into the silicon [9], adversely impacting the open-circuit voltage V_{OC} and fill factor *FF* of finished devices [10].

In this work, we present a thorough investigation of the correlation between contact resistivity and the process conditions, such as the evaporation rate, sintering temperatures, and sample surface doping concentration.

The characteristics of Si/Al contacts (both n+ and p+ doped Si) are then compared against literature values for passivated contacts via 3D simulations to demonstrate the idealised efficiency of each contacting technology in regards to solar cell efficiency.

II. Experimental Details

The test structures are fabricated using four-inch mechanically polished monocrystalline, (100) orientation, p-type, Czochralski (Cz), 100 Ω·cm wafers. The diffusion was performed using a high temperature quartz furnace tube with $POCl_3$ vapour as the dopant source with a 2 hour 1000 ^{o}C furnace anneal drive-in step. The samples were then etched back to provide a range of surface concentrations, which were determined by measuring the diffusion profile using electrochemical capacitance-voltage (ECV) measurements. For the samples that were not measured directly by ECV, the dopant profile was assumed to be identical with that measured for the non-etched sample but neglecting the first x µm of the profile. The depth x is selected such that the calculated sheet resistance of the profile equaled the measured sheet resistance of the sample. The measured and calculated profiles are plotted in Fig. 1.

The samples were given a dip in 5% hydrofluoric acid and blown dry immediately prior to metal evaporation. Metal evaporation was performed in a vacuum bell jar, using a disposable tungsten boat loaded with Al pellets (5N purity). The vacuum jar is evacuated to 5×10^{-5} Torr using an oil vacuum roughing pump and a cryopump with precautions to prevent back streaming of oil into the chamber via

This program has been supported by the Australian Government through the Australian Renewable Energy Agency (ARENA). Responsibility for the view, information or advice expressed herein is not accepted by the Australian Government.

This work was performed at ANU under a research contract for Trina Solar and through a joint research project between Trina Solar and the Solar Energy Research Institute of Singapore (SERIS). SERIS is sponsored by the National University of Singapore and Singapore's National Research Foundation through the Singapore Economic Development Board. This work is supported by the National High-Tech R&D Program (863 program) of the Ministry of Science and Technology of China under project number 2012AA050303.

K. C. Fong, T. C. Kho, A. Fell, E. Franklin, N. Zin, A. W. Blakers, T. Ratcliff, M. Stocks, J. Bullock and E.C. Wang are with the Australian National University, Acton, 0200, Australia (Corresponding author's e-mail: kean.fong@anu.edu.au).

Keith R. McIntosh is the director of PV Lighthouse, Wollongong, Australia. (email: krmcintosh@gmail.com).

electronically controlled valves. The deposition rate is measured using a gold coated crystal (6MHz by Inficon). The boat power is varied between 600 W and 800 W for the evaporation step which corresponds to a deposition rate of 10 Å/s to 60 Å/s respectively and evaporation is stopped when the Al source is depleted, determined by the deposition rate dropping below 3 Å/s. The thickness of evaporated Al on the samples is approximately 1 µm.

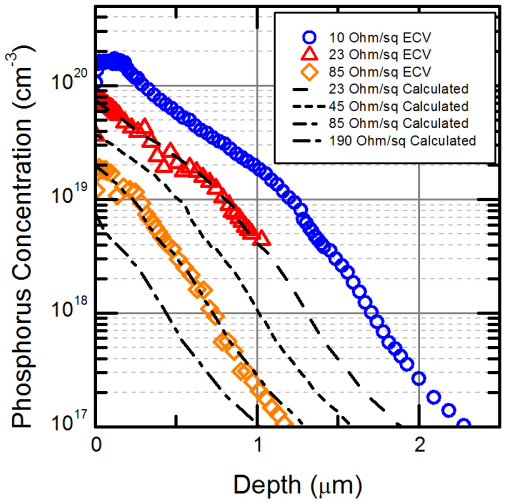

Figure 1: Doping profile of samples after etch-back. Comparison between measured profiles and profiles calculated from sheet resistance shows good agreement.

The contact between metal and semiconductor is characterised by its contact resistivity ρ_c ($\Omega \cdot cm^2$) measured by the transmission line method (TLM) [9, 11]. The TLM structure used is illustrated in Fig. 2, with pad length, *l* measuring 2 mm, width, *W* measuring 6 mm and gap spacing (d_x) ranges from 13 µm to 303 µm. The structures are formed by standard photolithography followed by an etch using a metal etch solution consisting of H_3PO_4:H_2O:HNO_3 at a ratio of 20:4:1. Individual TLM sets are physically cut out by dicing saw. A Keithley 2425 sourcemeter was used to perform 4 point measurement to eliminate systemic error of including the contact resistance between the probe and Al pad in the resistance measurements.

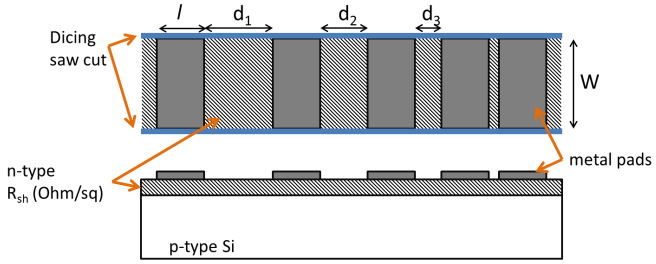

Figure 2: Illustration of TLM structure used.

III. RESULTS AND DISCUSSION

We investigated the effect of sintering temperature using a baseline evaporation recipe with the shutter opened during the Al pellet melting phase and using a boat power of 600 W, providing a maximum deposition rate of 10 Å/s. A set of samples were prepared as described in Section II and then sintered at temperatures ranging from 230 °C to 380 °C for 30 minutes in forming gas (FGA) (5% hydrogen 95% nitrogen). The results are presented in Fig. 3. The results published by Schroder [9] and Yu [8], which were attained by depositing Al with an electron beam gun and annealing between 400-500 °C, are also included for comparison. The contact resistivity prior to sintering is too high to be measured reliably with TLM, and is excluded from the data. Compared to the samples sintered at 380 °C, the contact resistivity for samples sintered at 230 °C is two orders of magnitude higher, and the contact resistivity for samples sintered at 280 °C is one order of magnitude higher.

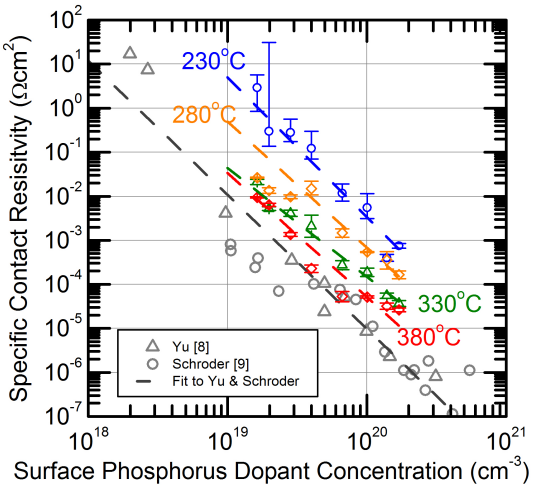

Figure 3: Contact resistivity results for 600 W boat power with shutter always opened. Sintering was performed at designated temperature for 30 minutes.

It was observed that while it takes ~10 seconds for the tungsten boat to glow red, the pellets require a significant amount of time to melt and deposition to be detectable by the crystal sensor; specifically, it took 90 s, 45 s, and 35 s for boat powers of 600 W, 700 W and 800 W, respectively.

By keeping the evaporation shutter open, it is possible that contaminating substances from the exposed tungsten boat or surface contaminants from the Al metal are deposited onto the silicon samples prior to the Al pellets evaporating, forming an interfacial layer at the metal-silicon interface. To protect the samples from contaminants during this initial warm-up phase, the evaporation recipe was modified to keep the shutter closed until the Al pellets start to evaporate. Two sets of diffused samples were prepared and metal evaporation was performed at 600 W and 800 W. The sample preparation method is as described in Section II, and sintering was performed between 230 °C and 380 °C for 30 minutes in a FGA ambient. TLM measurements were performed before and after the sintering step.

The results are presented in Figs. 4 and 5. For both 600 W and 800 W, the lowest contact resistivity occurs when there is no sintering. Contact resistivity with no sintering, and at

higher doping concentration is significantly lower when a higher boat power is used. The contact resistivity becomes higher when the samples are subjected to sintering, but does not exceed the values measured in Fig. 3. The reason for having lowest contact resistivity without sintering is unknown, but a possible explanation is that the contact resistivity between Si and Al is lower than the contact resistivity between Si and Si/Al alloy which forms as the interfacial layer when sintered even below the eutectic temperature.

The temperature of the samples during metal evaporation was determined to have not exceeded 80°C by direct evaporation of Al onto temperature sensitive strips with permanent color indicators.

The measured contact resistivity for the unsintered samples with Al deposition power of 800 W is the lowest published to date for the given surface dopant concentration, and is roughly an order of magnitude lower than values published in [8] and [9]. This result is extracted from three sets of TLM structures which were processed simultaneously. The measurements of resistance versus pad spacing for all three sets and the linear fit are presented in Fig. 6, and the extracted parameters presented in Table 1.

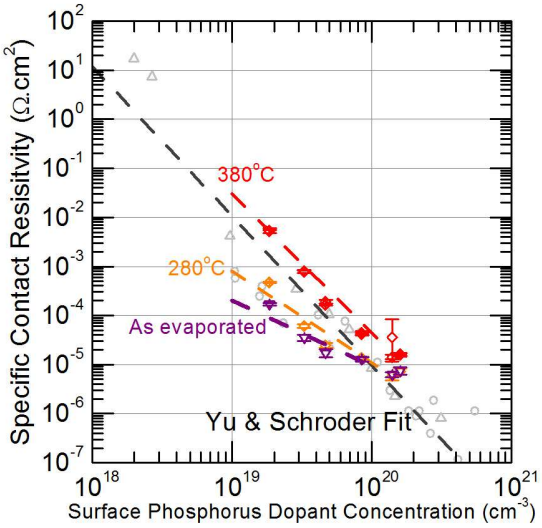

Figure 4: Contact resistivity for 600 W boat power, 120 s shutter delay. Sintering was performed at designated temperature for 30 minutes.

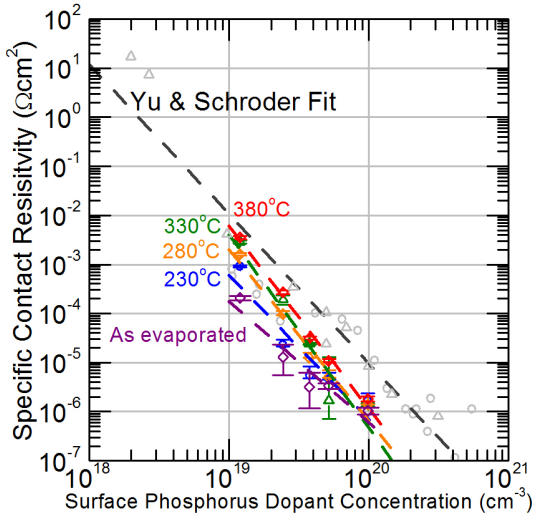

Figure 5: Contact resistivity for 800 W boat power, 60 s shutter delay. Sintering was performed at designated temperature for 30 minutes.

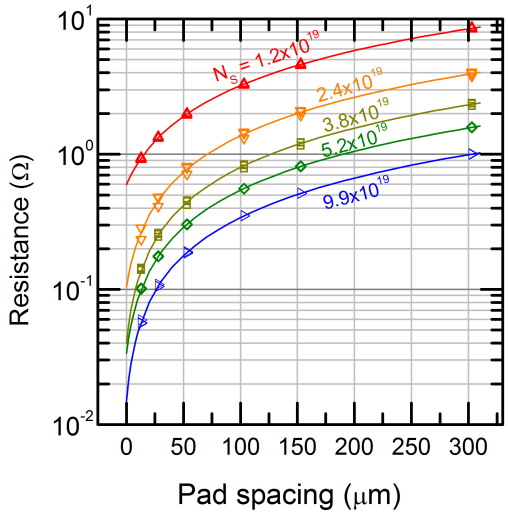

Figure 6: Resistance vs TLM pad separation for 'As evaporated' 800W deposition of Fig. 5 for different surface doping concentration, N_S. The fit is a linear fit but presented in a semi logarithmic scale to enable visibility of the intercept at x=0.

Table 1: Extracted TLM parameters for 'As evaporated' 800W deposition of Fig. 5.

	Surface doping concentration (cm^{-3})				
	$9.9x10^{19}$	$5.2x10^{19}$	$3.8x10^{19}$	$2.4x10^{19}$	$1.2x10^{19}$
R_{sheet} (Ω/□)	19.5	30.6	45.6	75.9	157.1
$2*R_C$ (Ω)	0.015	0.033	0.040	0.103	0.597
L_T (μm)	2.3	3.3	2.6	4.1	11.4
ρ_C (μΩ·cm^2)	1.04	3.31	3.16	12.75	204.2

IV. IMPLICATION TO CELL EFFICIENCY

Solar cell design always contains a trade-off relating to the contact area. Increasing the contact area introduces more recombination and shading losses (for front contact devices) whereas decreasing the contact area introduces greater resistive losses due to contact resistance and current crowding. Thus, the low contact resistivity presented above could lead to a reevaluation of the optimal contact area in high-efficiency cells. We demonstrate this optimisation and its ramifications for cell efficiency using 3D simulation with Quokka [12]. The unit cell used for this simulation as illustrated in Fig. 7 is an idealised structure with fully contacted but unshaded front emitter, with locally diffused rear point contact as is typical of Passivated Emitter Rear Locally Diffused (PERL) solar cells, and locally diffused Interdigitated Back Contact (IBC) cells. The bulk recombination is calculated using the intrinsic lifetime model for a bulk resistivity of 100 Ω·cm [13], substrate thickness of 230 μm, and a generation profile calculated using the AM1.5g spectrum with an optimised anti-reflection coating, yielding 42 mA/cm^2 of photogeneration.

Since the simulation is designed with the intention of maximising the sensitivity to the contact recombination and resistive losses, all surfaces are regarded as ideal (zero recombination) except for the locally diffused contact region, and no bulk Shockley-Read-Hall (SRH) recombination is included.

The rear contact fraction is optimised for each combination of ρ_c and J_0 in the simulation by fixing the dot size to 20 × 20 μm squares and varying the pitch of the contact-to-contact spacing. The choice of the 20 × 20 μm contact size is due to it being achievable by photolitography, laser processing [4], and within achievable range for high resolution ink-jet printing[14].

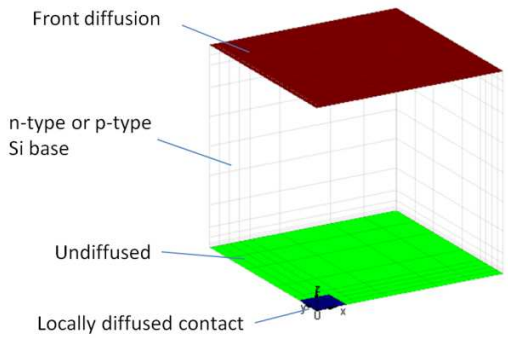

Figure 7: Geometry of the simulation unit cell, featuring a locally diffused rear point contact. Front refers to the illuminated side. The contact size is fixed at 20 x 20 μm, and the unit cell dimensions in x- and y-direction are varied to find the optimum efficiency.

The simulation is performed for both 100 Ω·cm n-type and p-type wafers where the locally diffused contact is N+ doped and P+ doped respectively.

The bulk resistivity is high enough that it is essentially considered to be intrinsic silicon under operating conditions, and therefore nullifies the differences of the diffused regions being either a back surface field (BSF, same doping polarity as the bulk Si), or emitter (opposite doping polarity to bulk Si). Therefore, the presented results for both n+ and p+ contacts applies irrespective of it being a BSF or emitter, which is particularly useful in its interpretation for IBC devices.

Results of the simulation are presented in Figs. 8 & 9, where the rainbow color contours represent the maximum efficiency found by optimization of the unit cell pitch. The resulting optimal pitch is also represented as an overlaid yellow/orange dotted line contour. Therefore, for any position within the x-y axis of the plot, there exist an optimal efficiency, and an optimal pitch used to achieve it. Such an approach to efficiency potential via multidimensional simulations of an idealised structure was similarly employed in [15, 16] using equivalent circuit models, and in [17, 18] with consideration of crowding effects.

The n+ contact results from this work are superimposed into Fig. 8, where the J_0 values used for this region are obtained experimentally by photoconductance decay measurement on the samples prior to its preparation for TLM measurements. The results are compared to several passivated contacts [17-19]. The difference between highest efficiency attainable for Si/Al contact and passivated contacts are small, which fall within the efficiency range of 27.8 -28.2 %.

A similar observation is made for p+ contacts as presented in Fig. 9. The Si(p+)/Al contact data is from reference [6] and was performed using an identical process as described for Fig. 5 using 800 W deposition power, and 230 ^{o}C sintering in FGA. Results for Si(p+)/Al contacts at higher surface dopant concentration as plotted in Fig. 9 was extracted by combining measured J_0 results from [20] and converting the measured surface doping concentration to contact resistivity by using a power fit to Schorder's data in [9]. Results of passivated contacts from literature [19, 21] are also superimposed over the contour plot. The best results for direct Si/Al contact and passivated contacts fall between 27.4 – 27.8 % efficiency.

In both Figs. 8 and 9 the efficiency contours plateau at a contact resistivity less than 10^{-4} Ω·cm^2, indicating that the resistive loss at the contact no longer limits the device efficiency. It is rather the internal bulk resistance and recombinative losses that dominate the losses.

As was briefly noted above, this idealised simulation case highlights the differences between the contact properties. If realistic values of surface and bulk recombination are then included, it will further reduce the differences between optimal efficiency for the different contact technologies.

By comparing the data points of different contact technologies on the same plot, we are assuming negligible difference in optical performance of the different rear contact stacks. This is a reasonable approximation since intermediate layers on most passivated contact stacks are very thin and weakly absorbing to long wavelength light.

Unless a self-aligned technique is used for diffusion and contact opening, perfect alignment such as is assumed for the simulation is impossible. A fabricated device would require the contact opening to be smaller than the diffused region by an amount reasonable to the alignment tolerance of the tool used. To interpret Figs. 8 and 9 for a device fabricated with contact opening smaller than the diffused region (such as is

done in [6]), then the worst case assumption is to assume the unpassivated J_0 for the entire diffused area, and an increase in the contact resistivity by the ratio of contact:diffused area. This would result in data points being shifted towards the right side of the contour plot. For both the n+ and p+ contacts, the contact resistivity for heavily diffused Si/Al contacts is sufficiently low that an increase by a factor of 2 in contact resistivity will not decrease its optimal efficiency.

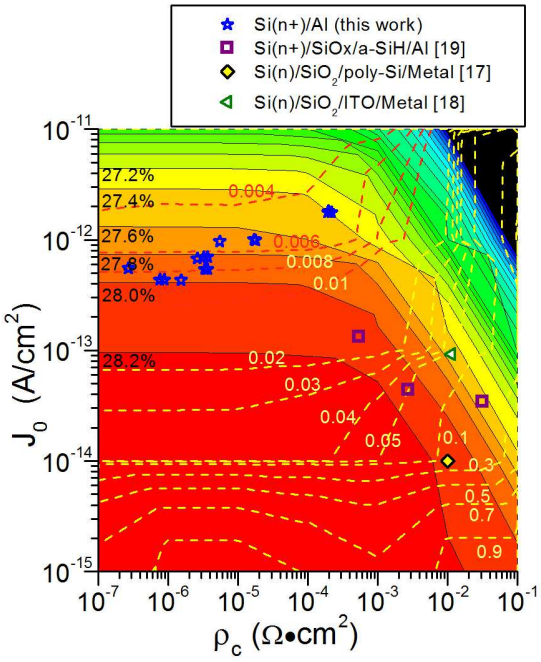

Figure 8: Optimal efficiency for rear locally diffused n+ contacts as would be the case for IBC or n-type PERL. The rainbow colored contour plot is efficiency and the yellow/orange dotted line is the optimal contact fraction to achieve it (eg: 0.01 representing 1% rear contact area).

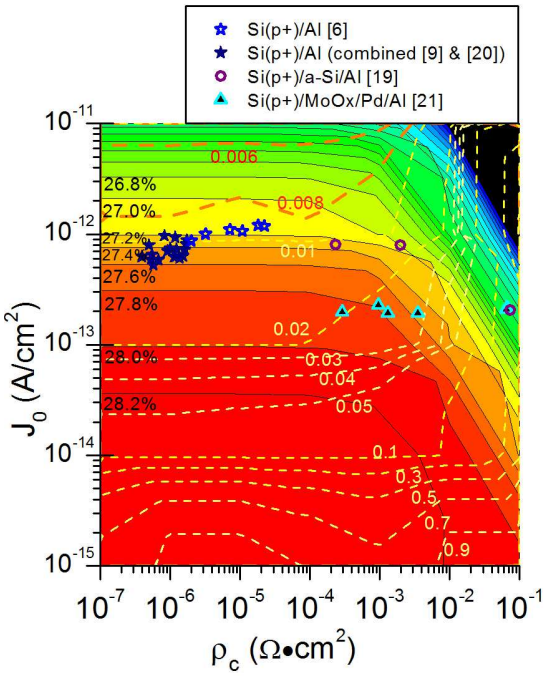

Figure 9: Optimal efficiency for rear locally diffused p+ contacts as would be the case for an IBC or p-type PERL cells. The rainbow colored contour plot is the efficiency and the yellow/orange dotted line is the optimal contact fraction to achieve it (eg: 0.01 representing 1 % rear contact area).

V. CONCLUSION

The results presented in Table 1 for Al contact resistivity on phosphorus doped Si are the lowest values presented to date at their respective doping concentration, and we demonstrated that very low contact resistance is achieved without the need of a sintering step.

The obtained results are compared to passivated contact technology via 3D simulation of an ideal unit cell with locally diffused contacts. The conclusion from these simulations is that direct Si/Al contacts and the best published results for passivated contacts (amorphous Si for n+ and and Molybdenum oxide contacts for p+) appear to have efficiency above 27.4%. Therefore, for a practical device of ~25% efficiency, these contact techniques will not be the limiting factor at optimal contact fractions.

From a fabrication practicality point of view, in order to take advantage of the very low contact resistivity achievable via evaporated Al, advanced techniques which provide fine features with precise alignment are required. Such limitations are not fundamental limits and can be alleviated by advancement in technology such as adoption of high resolution ink-jet printing or laser patterning / doping.

REFERENCES

[1] A. Cuevas, P. A. Basore, G. Giroult-Matlakowski, and C. Dubois, "Surface recombination velocity of highly doped n-type silicon," *Journal of Applied Physics*, vol. 80, pp. 3370-3375, 1996.

[2] G. A. Armin, *Crystalline Silicon Solar Cells: Advanced Surface Passivation and Analysis*. Sydney: Centre for Photovoltaic Engineering, University of New South Wales, Sydney, Australia, 1999.

[3] A. Wang, J. Zhao, and M. A. Green, "24% efficient silicon solar cells," *Applied Physics Letters*, vol. 57, pp. 602-604, 1990.

[4] A. W. Blakers, A. Wang, A. M. Milne, J. Zhao, and M. A. Green, "22.8% efficient silicon solar cell," *Applied Physics Letters*, vol. 55, pp. 1363-1365, 1989.

[5] J. Zhao, A. Wang, P. Altermatt, and M. A. Green, "Twenty-four percent efficient silicon solar cells with double layer antireflection coatings and reduced resistance loss," *Applied Physics Letters*, vol. 66, pp. 3636-3638, 1995.

[6] E. Franklin, K. Fong, K. McIntosh, A. Fell, A. Blakers, T. Kho, D. Walter, D. Wang, N. Zin, M. Stocks, E.-C. Wang, N. Grant, Y. Wan, Y. Yang, X. Zhang, Z. Feng, and P. J. Verlinden, "Design, fabrication and characterisation of a 24.4% efficient interdigitated back contact solar cell," *Progress in Photovoltaics: Research and Applications*, pp. n/a-n/a, 2014.

[7] F. Heinemeyer, C. Mader, D. Münster, T. Dullweber, and R. Brendel, "Inline high-rate thermal evaporation of aluminium for novel industrial solar cell metallization," 25th *EU PVSEC Valencia*, pp. 2066-8, 2010.

[8] A. Y. C. Yu, "Electron tunneling and contact resistance of metal-silicon contact barriers," *Solid-State Electronics*, vol. 13, pp. 239-247, 1970.

[9] D. K. Schroder and D. L. Meier, "Solar cell contact resistance; A review," *Electron Devices, IEEE Transactions on*, vol. 31, pp. 637-647, 1984.

[10] K. C. Fong, "Fabrication and characterisation of elongate solar cells," PhD Thesis, The Australian National University, Canberra, 2012.

[11] H. H. Berger, "Contact resistance and contact resistivity," *Journal of The Electrochemical Society*, vol. 119, pp. 507-514, 1972.

[12] A. Fell, "A free and fast three-dimensional/two-dimensional solar cell simulator featuring conductive boundary and quasi-neutrality approximations," *Electron Devices, IEEE Transactions on*, vol. 60, pp. 733-738, 2013.

[13] A. Richter, F. Werner, A. Cuevas, J. Schmidt, and S. W. Glunz, "Improved parameterization of Auger recombination in silicon," *Energy Procedia*, vol. 27, pp. 88-94, 2012.

[14] L. Zhongtian, C. Ran, Y. Yu, Z. Wei, W. Xi, I. Perez-Wurfl, and A. Lennon, "Patterning and metallization of silicon solar cells by inkjet-printed functional ink on a photoresist layer," in *Photovoltaic Specialist Conference (PVSC), 2014 IEEE 40th*, 2014, pp. 2499-2501.

[15] A. Fell, S. Surve, E. Franklin, and K. J. Weber, "Characterization of laser-doped localized p-n junctions for high efficiency silicon solar cells," *Electron Devices, IEEE Transactions on*, vol. 61, pp. 1943-1949, 2014.

[16] J. Bullock, D. Yan, and A. Cuevas, "Passivation of aluminium–n^+ silicon contacts for solar cells by ultrathin Al_2O_3 and SiO_2 dielectric layers," *Physica Status Solidi (RRL) – Rapid Research Letters*, vol. 7, pp. 946-949, 2013.

[17] F. Feldmann, M. Bivour, C. Reichel, M. Hermle, and S. W. Glunz, "Passivated rear contacts for high-efficiency n-type Si solar cells providing high interface passivation quality and excellent transport characteristics," *Solar Energy Materials and Solar Cells*, vol. 120, Part A, pp. 270-274, 2014.

[18] D. L. Young, W. Nemeth, S. Grover, A. Norman, H.-C. Yuan, B. G. Lee, V. LaSalvia, and P. Stradins, "Carrier selective, passivated contacts for high efficiency silicon solar cells based on transparent conducting oxides," *Energy Procedia*, vol. 55, pp. 733-740, 2014.

[19] J. Bullock, A. Cuevas, D. Yan, B. Demaurex, A. Hessler-Wyser, and S. De Wolf, "Amorphous silicon enhanced metal-insulator-semiconductor contacts for silicon solar cells," *Journal of Applied Physics*, vol. 116, pp. -, 2014.

[20] D. Yan and A. Cuevas, "Empirical determination of the energy band gap narrowing in p+ silicon heavily doped with boron," *Journal of Applied Physics*, vol. 116, pp. -, 2014.

[21] J. Bullock, A. Cuevas, T. Allen, and C. Battaglia, "Molybdenum oxide MoOx: A versatile hole contact for silicon solar cells," *Applied Physics Letters*, vol. 105, pp. -, 2014.

Kean Chern, Fong received his bachelor of engineering from Multimedia University, Malaysia in 2005, and his PhD in photovoltaics from Australian National University in 2012 on the topic of fabrication and characterization of photovoltaic cells.

He was a Test Software Engineering at Intel Corporation from 2005 to 2008, and is currently a Research Fellow at the Australian National University. He has numerous publications in the field of silicon solar cell fabrication, characterization and simulation. His areas of interest include high efficiency silicon solar cells particularly interdigitated back contact (IBC) solar cells, surface passivation, device characterization, loss analysis and modelling.

Dr. Kean Chern Fong is an alumnus of the Australian Endeavour Awards, who received the post-graduate Endeavour Scholarship in 2008.

Evan Franklin received the PhD degree from the Australian National University, Canberra, Australia in 2006 on the design, fabrication and characterisation of silicon solar cells. He has authored numerous conference and journal papers on solar cell modelling and fabrication, and on laser processing for silicon photovoltaics. His current research interests include modelling and manufacturing of interdigitated back contact cells and other high efficiency concepts, the development and incorporation of laser processes suitable for industrial PV manufacturing, and the integration of PV systems into the electrical power network.

Andreas Fell received the PhD degree in physics from the University of Konstanz, Germany in 2010. From 2006 - 2011 he was a researcher at Fraunhofer ISE, Freiburg, Germany. He joined the Australian National University in 2011 as a research fellow for the development of laser processes for silicon solar cells. His current research scope expands on multidimensional solar cell device modeling.

Teng Choon, Kho received BSc and BEng degree in chemistry and electronic engineering in 2010 at the Australian National University. He is currently perusing his Ph.D. degree at the Australian National University.

From 2010 to 2014, he was a Research Assistant at the Australian National University involved in numerous projects. His research interest includes modelling, optimizing and

development of silicon solar cells. He is a key member of the team who fabricated the 24.4% efficiency IBC solar cell at ANU in 2013.

Mr Teng Choon Kho is a recipient of the ANU Australian Postgraduate Award. He has received multiple research scholarship awards during his undergraduate studies in 2008 and 2009.

Thomas Ratcliff received his B Eng.(Hons) in 2009 from the Australian National University, where he is currently completing his PhD program.
His research has focussed on advanced doping techniques, including ion implantation, for back contact Si solar cells.

Ngwe Zin received a MSc degree from Nanyang Technological University, Singapore in 2005 and a PhD degree from Australian National University (ANU) in 2011. He was a postdoctoral researcher at ANU from 2011 to 2012, and is undertaking postdoctoral research fellowship from 2013 till present. His research interests are development of novel structures, measurements, device fabrication, characterisation, analysis and modelling in the field of high efficiency silicon solar cells. He is a recipient of Australian Renewable Energy Agency (ARENA) funded fellowship.

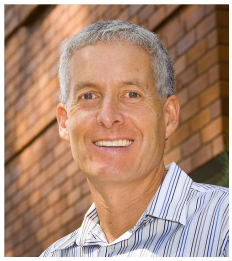

Professor Andrew Blakers is a Professor of Engineering at the Australian National University (ANU). His research interests are in the areas of photovoltaic and solar energy systems; silicon solar cell technology, concentrator solar cells, components and systems; and sustainable energy policy.

Professor Blakers has held a Radio Research Board Postdoctoral Fellowship, an ARC Queen Elizabeth II Fellowship, a Humboldt Fellowship and an ARC Senior Research Fellowship. He was appointed to the academic staff of the ANU in 1991 and reached the rank of Professor in 1999. Projects under the supervision of Professor Blakers have brought in $100 million to ANU. Professor Blakers is well known as a commentator on energy and greenhouse issues. He is a Fellow of the Australian Academy of Technological Sciences and Engineering, the Australian Institute of Physics and the Australian Institute of Energy. He is a life member of the International Solar Energy Society and the Australian Conservation Foundation.

Keith R. McIntosh is the director of PV Lighthouse, a company that develops and hosts simulation software for photovoltaic engineers. He received the PhD degree in electrical engineering in 2001 from the University of New South Wales, Sydney.

From 2001 to 2004, he was with SunPower Corporation, Sunnyvale, CA, USA, where he was a core member of the team that developed the A-300 high-efficiency rear-contact solar cell. From 2005 to 2011, he was a Research Fellow with the Australian National University, Canberra, Australia, where he led a research group that focused on the optics and recombination in silicon solar cells. Keith founded PV Lighthouse in 2011.

James Bullock received B.S and B Eng (Hons.) degrees from the Australian National University in 2012. He is currently working towards his PhD in Engineering at the same university.

Matthew Stocks received his PhD degree in Engineering from the Australian National University in 2002 on high efficiency multicrystalline solar cells. From 2003 through 2012, he transferred SLIVER cell technology from the ANU into commercial manufacture, leading the cell research and development activities and culminating in the role of Chief Technologist of Transform Solar from 2008-2012.

His current interests include modelling, characterisation and implementation approaches for high efficiency devices including IBC solar cells and tandem devices based on silicon and the transfer of university developments into industrial solar cells.

Er-Chien Wang received his BEng (Hons.) in 2008 from the University of Canterbury and PhD degree from The Australian National University in 2013. During his PhD degree, his research was focused on surface treatments for both antireflection and light trapping applications, novel solar cell structure designs and improvement on the nanoimprint lithography process. He is currently undertaking postdoctoral research in the field of IBC solar cells.